Applied Mathematical Modelling 69 (2019) 93–112

Contents lists available at ScienceDirect

Applied Mathematical Modelling

journal homepage: www.elsevier.com/locate/apm

Valuating fire suppression risk data

Alex T. Masarie [a,*], Yu Wei [a], Erin J. Belval [c], Matthew P. Thompson [c], Iuliana Oprea [b], Maryam Tabatabaei [a], Dave E. Calkin [d]

[a] *Department of Forest and Rangeland Stewardship, Colorado State University, Fort Collins, CO, United States*
[b] *Department of Mathematics, Colorado State University, Fort Collins, CO, United States*
[c] *USDA-FS Rocky Mountain Research Station, Fort Collins, CO, United States*
[d] *USDA-FS Rocky Mountain Research Station, Missoula, MT, United States*

ARTICLE INFO

Article history:
Received 11 June 2018
Revised 26 October 2018
Accepted 29 November 2018
Available online 8 December 2018

Keywords:
GIS data analysis
Ordinary differential equation
Fire management
Math model

ABSTRACT

Efficient and effective wildland fire response requires interregional coordination of suppression resources. We developed a mathematical model to examine how scarce resources are shared. Best-fit models describe regional resource allocation according to driving risk factors. By regressing a linear system of ordinary differential equations with GIS-data for demand predictors like suppression resource use, ongoing fire activity, fire weather metrics, accessibility, and population density onto pre-smoothed Resource Ordering Status System (ROSS) wildfire personnel and equipment requests, we fit a national scale model. We report statistical properties of the best-fit parameters and indicate how these findings might be interpreted for personnel and equipment sharing by examining test cases for national, central/southern Rockies, and California interregional sharing. Abrupt switching behavior across medium and high alert levels was found in test cases for national, central/southern Rockies, and California interregional sharing.

1. Introduction

The United States Federal government has been investing significantly into fire suppression every year; (USDA, The Rising Cost of Wildfire Operations 2015) explains we expect to face extended periods of elevated fire risk more frequently in the future due to factors such as climate change and rapid expansion of wildland urban interface (WUI). Wildfire is a natural hazard and mitigating fire risk through expensive firefighting is often a top priority. By 2025, USDA [1] projects for every two dollars spent on fire, only one will remain in the budget for all the Forest Service's non-fire work combined – i.e. forest stand management and restoration, eco-tourism, etc. Where human structures are situated in forested surroundings, wildfire suppression workloads are on the rise. USDA [1] finds current fire seasons are an average of 78 days longer than in 1970. These extra work days often involve transporting firefighters and equipment long distances from home bases to fire incidents or between incidents. It is important to identify and study key factors influencing the allocation of these firefighting resources, particularly during times of elevated fire activity when resources are scarce. A shortage of resources can manifest as high dollar costs from escaped fires.

Fire suppression is often triggered by smoke detections or activated in response to wildfire monitoring systems. Containment rates of initial attack fires are known to be high in the US; Calkin et al. [2] reported between 97% and 99% successful

* Corresponding author.
E-mail addresses: Alex.Masarie@colostate.edu (A.T. Masarie), yu.wei@colostate.edu (Y. Wei), juliana@math.colostate.edu (I. Oprea).

https://doi.org/10.1016/j.apm.2018.11.049
0307-904X/

Table 1
Fire suppression resources.

$R =$	COLOR	Terrestrial	$R =$	COLOR	Aerial
1		Firefighter Type 1 ($FFT1$)	5		"Helitak" ($Helicopter$)
2		Firefighter Type 2 ($FFT2$)	6		Various models ($Airtanker$)
3		Types 1-6 ($Engine$)	7		Smokejumpers ($SMKJ$)
4		Types 1-3 ($Dozer$)	($Italics$) *ROSS archive data mining strings*		

Table 2
United States geographic area coordination centers.

Domain partition: $\Omega = \bigcup_g \Omega_g$ is disjoint $G \neq g \Rightarrow \Omega_G \cap \Omega_g = \emptyset$		
G=	*CODE*	*Name, additional zones (notes)*
1	**EACC**	Eastern Area Coordination Center, 2 sub-zones
2	**RMCC**	Rocky Mountain Coordination Center
3	**SWCC**	Southwestern Coordination Center
4	**EGBCC**	Eastern Great Basin Coordination Center, 2 sub-zones
5	**WGBCC**	Western Great Basin Coordination Center
6	**SACC**	Southern Area Coordination Center, 2 sub-zones
7	**AKCC**	Alaskan Coordination Center, 3 sub-zones
8		Hawaii, as part of NOCC
9	**NWCC**	Northwestern Coordination Center
10	**NRCC**	Northern Rockies Coordination Center, NRCC
11	**NOCC**	Northern Operations (Northern California)
12	**SOCC**	Southern Operations (Southern California)

(Latitude, longitude) data pairs (*lx, ly*) in degrees NAD83.

containment. The remaining 1%–3% escape initial attack and continue to grow as uncontained fires entering a suppression response period called the extended attack. Large fires, those 300 ha or more in size, require adaptive management tactics that vary based on fire growth, behavior, and danger they present to human infrastructure, and ecological values for example, forest health and species habitat USDA [1]. During periods of elevated fire activity, management may be required to oversee operations on multiple, simultaneous fires within a region. In either initial or extended attack, a fire manager might decide to summon extra help from the national pool of resources – see Table 1 for examples – to stop the spread of a given fire Interagency Red Book [3].

We know from [4] that efficient and effective wildfire response entails system-level coordination. Beyond the local crews and equipment, a manager can requisition any resource they need via the Resource Ordering Status System (ROSS). Most large fire requests are processed through ROSS. Therein the request is marked as "filled" or remains "unable-to-be-filled" subject to current availability within the national pool of resources. This resource demand and sharing database is central to our analysis of demand during natural hazard mitigation for wildfires in the United States – see Table 2 for examples of wildland fire regions.

There are five levels of national preparedness level in fire suppression (PL) that rank overall fire activity and resource use (National Interagency Mobilization Guide, Chapter 20). They are updated daily. For example, at Preparedness Level 3:

> "Two or more Geographic Areas are experiencing wildland or prescribed fire activities requiring a major commitment of National Resources. Additional resources are being ordered and mobilized through NICC [National Interagency Command Center]. Type 1 and 2 Incident Management Teams are committed in two or more Geographic Areas and crew commitment national is at 50%."

PL 4 is notable for increasing the number of Geographic Areas to three and 60% national commitment of crews and managers. PL 5 moves to 80% commitment and is specific to "the potential to exhaust all agency fire resources." Our analyses were designed to contrast high alert ($PL = 4$ *or* 5) versus normal status days ($PL = 2$ *or* 3) – no analyses were performed on the days with $PL = 1$. Wildfire preparedness alerts are also reported by each of the twelve, individual Geographic Areas in the U.S. as well.

We surveyed the literature for a working list of viable risk factors that matter for wildfire hazard mitigation. Our research indicated fire fighter experience, past collaborations, and personal factors [6], fire weather and behavior variables [7], and management considerations such as: resource effectiveness upon arrival [8], dispatch and coordination of suppression resources [9,10], Incident Command Teams that direct operations [11], and variability among individual decision-makers [12,13]. We tested forty-five viable risk factors – eleven spatiotemporal factors are described in Table 3 and an additional thirty-four factors derived from these are summarized in Table 4.

Ordinary differential equation (ODE) models are designed to explain how a system would iterate from initial states through a series of discrete time steps according to known system dynamics. Moreover, ODE system models have been developed to describe many types of spatial dynamics from the transmission of infection diseases to predator–prey interactions [5]. While we found no previous work of using ODE systems in fire resource allocation, some researchers have used

Table 3
List of viable factors in study's risk database.

ODE model #	Name	**Description of variable:** [Units]	Additional notes	*Interpolation method* ⋯ **Further reference**
1	*CONSTANT*	**Constant grid:** [all 1s]	Constant levels appear in many region/resource fits, it served as an extra calibration	*Generated one value per node*
2	*NOISE*	**Uniform i.i.d. noise:** [normalized 0–1]	Noise in best fit model leads to concern about unmodeled factors, personal bias	[a]*Such layers are recommended for grid-sizing, memory allocation in code*
3	*MODIS*	**Fire radiative power:** [Megawatt]	Moderate Resolution Imaging Spectroradiometer satellite fire detection, *MODIS MCD14ML 2011–2016* Filtered for confidence > 80% and actively burning pixels ≥ 2.02 km^2	*scatteredInterpolant.m splines to* max *of* ∼30 km *detection cluster radius* ⋯ **[MODIS 2016]**
4	*ERC*	**Energy release component of fuels:** [index 25–110]	Seasonal trend in fuel dryness potential. *UofI METDATA 2011–2016*	*Re*-gridded gERC found in [a].nc files from 585 × 1386 lat/lon ⋯ **[Abatzoglou et al. 2013]**
5	*FOD*	**Fire occurrence database:** [# of discoveries per PSA[a]]	Aggregated by 2016 Predictive Service Area (PSA), county-sized sub-units	Nearest neighbor to discovery count, sub-regional boundaries ⋯ **[Short 2017]**
6	*BI*	**Burning index flammability metric:** [index 0–110+]	Short–term trends in burning potential. *UofI METDATA 2011–2016*	Re-gridded gBI found in [a].nc files from 585 × 1386 lat/lon ⋯ **[Abatzoglou et al. 2013]**
7	*regionPL*	**Preparedness Level for regions:** [cat. 1,2,3,4,5]	Mined from IMSR NIFC 2011–2016	Nearest neighbor to PL category, boundaries – jump discontinuities ⋯ **[NICC.gov/ 2016]**
8	*WindVel*	**Magnitude of wind:** [m/s]	Both wind strengths and changes in direction are known to influence fire spread, especially when changes in wind indicate weather front movement	Re-gridded from wind vectors found in [a].nc files from 585 × 1386 lat/lon [a]Also used directly in ∂_t*WindVel* change from north ⋯ **[Abatzoglou et al. 2013]**
9	*geDIST* (*static*)	**Google Earth distance:** [easy 0.0 to 2.0 difficult road access]	Ad hoc selection of interregional roads, distance computations, scaled for curvature of earth, static	Interpolation on 9 km grids directly from .kml files
10	log *LSNITE*	**Log-transformed LandScan:** [log nighttime illuminance/km^2]	Grid cell samples median illuminance across adjacent cells, then scaled from brightest to darkest, static	Re-gridded high-resolution layer to 9 km per side ⋯ **[LandScan 2011]**
11	*COST*	**Ongoing expenditures Year-To-Date:** [log $]	*ICS-209 NIFC 2011–2014, 2015–2016 corrupt,* grouped by incident, transformed with log function	exponentialBumpGenr8r.m to incident log cost levels ⋯ **[NICC.gov/ 2016]**

[a] PSAs are smaller regions than Geographic Area Coordination Centers.

similar maximum likelihood frameworks like [[6]–[8]] in studying fire resource allocation. An ODE systems formulation is potentially suitable for fire suppression studies to uncover correlations among assignment data in ROSS and geographic information system (GIS) spatiotemporal risk factors.

In this study, we establish an inverse problem for a system of ODEs as a means of calculating the statistical likelihood of different behaviors over time and among regions. The model sorts GIS-based risk prognostics and produces likelihood estimates for numerical fit parameters as coefficients on linear interactions among their levels and rates of change. We assess the degree to which the best-fit system might be a so-called stiff system of ODEs, which tend to augment computational noise problems when making forward predictions [9].

While we explored wildfire resource ordering data specifically, our procedure generalizes to other multi-region natural hazard problems like flooding [10,11], storms [12], or even heat waves [13] that require extensive resource sharing and impact broad regions. This paper develops the model theory and uses 2011–2016 archive data to compute statistical likelihoods of the model's parameters. In the numerical version, we compared fire suppression assignments along the Rocky Mountain corridor spanning Wyoming, Colorado, and New Mexico (the Rocky Mountain and Southwest Coordination Areas) with California (the Northern and Southern California Coordination Areas). We ground the model and analysis in current policy, report best-fit parameters given historical data, and interpret coefficient estimates within the context of natural hazard mitigation resource demand, which is diagrammed in Fig. 1. Findings from the 2011–2016 data indicate more complicated models are necessary among the 151 high alert days, to achieve the same quality of fit as to the 405 normal status days. Findings

Table 4
Derived and composite GIS factors.
By ∂_t we mean a one-step backward difference, daily rate of change.

	MODIS 12 ∂_t*MODIS*	*ERC* 13 ∂_t*ERC*	*FOD* 14 ∂_t *FOD*	*BI* 15 ∂_t*BI*	*regionPL* 16 ∂_t *regionPL*	*WindVel* 17 ∂_t *WindVel*
geDIST (*static*)	18	19	20	21	22	23
	24	25	26	27	28	29
logLSNITE (*static*)	30	31	32	33	34	35
	36	37	38	39	40	41
∂_t*MODIS*	n/a	n/a	n/a	n/a	n/a	n/a
	n/a	42	n/a	43	n/a	n/a
∂_t*FOD*	n/a	n/a	n/a	n/a	n/a	n/a
	n/a	44	n/a	45	n/a	n/a

also indicate the demobilization or release of resource may cause inefficiencies for management of future fires. Our wildfire application-specific results might be used as a template for other allocation problems. For example, we expect this type of ODE model could also be applied to analyze the management of natural hazards such as flooding, storms, heat waves, or others where resources are required by multiple regions and could be enumerated such as in Table 1, multiply-connected regions exist like in Table 2, and a list of viable risk factors as in Table 3 could also be generated.

2. Materials and methods

2.1. Building and solving an inverse problem for ode model

The ODE model is for a collection of resources being shared amongst a collection of hazard management zones (HMZs). We use $R = 1,\ 2, \ldots,\ \#R$ to index different types of resources and $G = 1,\ 2, \ldots, \#G$ for HMZs. The union of HMZs forms a multiply connected domain $\Omega = \bigcup_{G=1,\ldots,\#G} \Omega_G$. Let $U_{R,G}(t)$ denote the hazard demand at time t for resource R in HMZ G. Our objective is to model demand data for resource R in HMZ G from some initial configuration at $t = T_0$ through $t = T_F$ based on viable risk information. To index different types of fire risk information we use = 1, 2,...; we will show how to use specific GIS layers in the next section.

Risk information is denoted $D_{i,G}(t)$ and considered exogenous, i.e. external, known data. We will use a *lowercase* typeset for parameters, coefficients, and sub-model indices. Our model equation has endogenous parameters a for risk weights, y for resource “reinforcing/releasing” from each HMZ, and z for cooperative “sharing.” Each parameter is specific to a resource R within HMZ G, but may be fit according to demand or risk data from the other resources and HMZs in the ODE system.

We modeled the unfolding of events during the hazard’s active duration as a gradual, day-to-day process occurring as resource needs become known. We created a system of coupled ODEs in time t to reflect ongoing regional changes in fire demand $U_{R,G}(t)$. The ODE system model component equations are

$$\begin{aligned} &\forall\ R = 1,\ \ldots,\ \#R \qquad \forall\ G = 1,\ \ldots,\ \#G \quad ODE(R,G):\ \frac{dU_{R,G}}{dt}(t) \\ &= \sum_{s \in Lag(R,G)} \left[\sum_{g=1}^{\#G} \left(y_{R,G,g}(t-s)\ U_{R,g}(t-s)\ +\ \sum_{i \in FACTORS} a_{i,R,G,g}(t-s) D_{i,g}(t-s) \right) \right. \\ &\left. + \sum_{r=1}^{\#R} z_{R,r,G}(t-s)\ U_{r,G}(t-s) \right]. \end{aligned} \tag{1}$$

The first line of Eq. (1) shows request rate data. For a given time t_0 when request rate data $\frac{dU_{R,G}}{dt}(t_0) > 0$, the HMZ G requests more resources of type R than in the previous time step. When $\frac{dU_{R,G}}{dt}(t_0) = 0$, the request level is constant from day to day. Some request rate data have $\frac{dU_{R,G}}{dt}(t_0) < 0$ meaning the number requests is lower than the previous time step. Risk data $D_{i,G}(t)$ and resource availability will influence these rates as multiple regional hazards develop at once leading to reallocation of resources.

The second line of Eq. (1) introduces an outer sum for lags. All parameters depend on $(t - s)$ where lag s refers to a recent time sample of risk information. The set $Lag(R,\ G)$ is used to specify which lags to sample for $ODE(R,\ G)$. Within the lag sum there a sum across sub-index g that steps through the $\#G$ HMZs in the system. Parameter $z_{R,G,\ g}(t - s)$ tells how request rates for resource R in HMZ G might depend on other HMZs g. Within the lag sum and the HMZ sum there is a risk *FACTORS* sum. We will say much more about the set *FACTORS*, but one target of the inverse problem is to learn about the composition of this set. Parameter $a_{i,R,\ G,\ g}(t - s)$ weights the ith risk information layer for resource R in HMZ G based on risk information in HMZ g.

The third line of Eq. (1) establishes an additional fire demand driver. Within the lag sum there is a resource sum. Sub-index r steps through the $\#R$ resources in the system. In contrast to $z_{R,G,\ g}(t - s)$ from the second line, the term $y_{R,r,\ G}(t - s)$

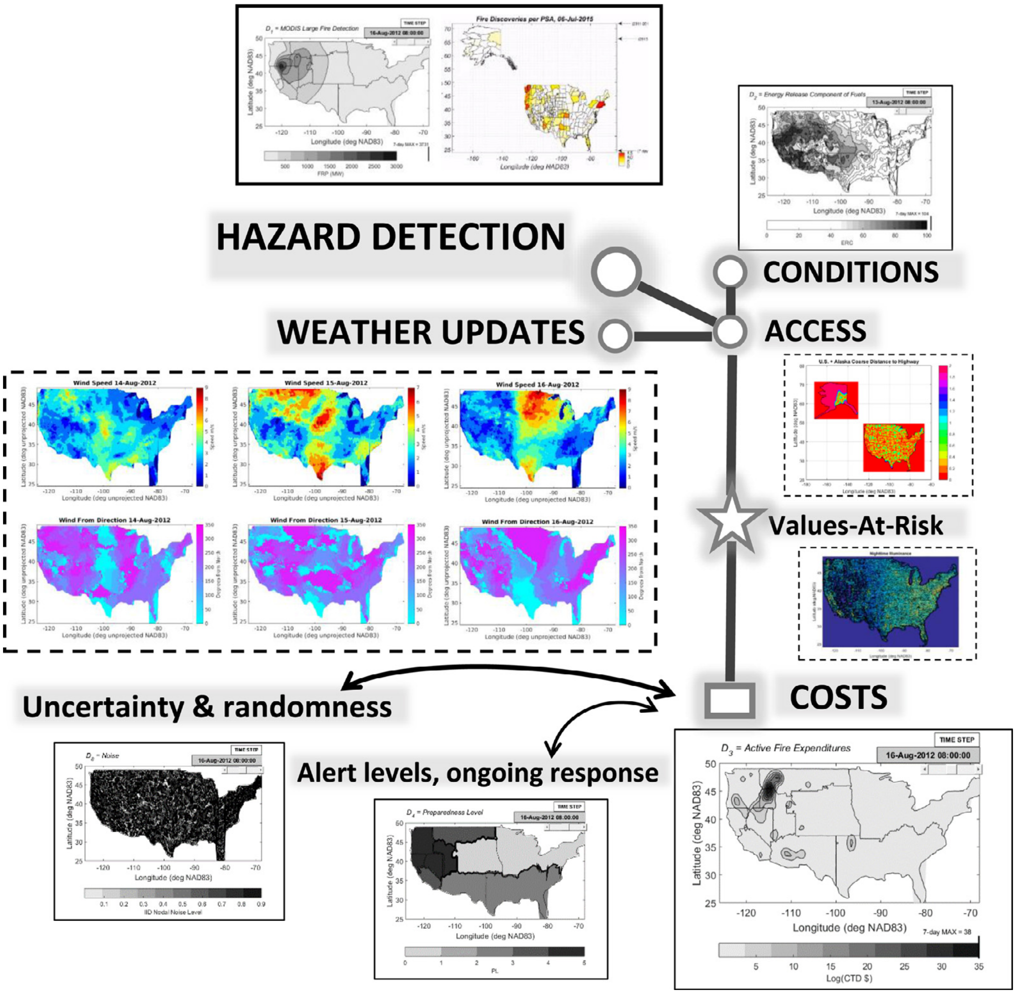

Fig. 1. Hazard framework and application area GIS examples.
Hazard detection sets off a chain of events that can lead to high dollar costs for risk mitigation. This study focused on hazards that can multiply across large spatial regions and have long management durations so as to warrant resource sharing. Within the boxes, GIS images show specific, viable factors we found in research literature for wildfire hazard mitigation, but the idea is our math-based method helps get organized. Natural hazard information requirements about weather updates, conditions, access, and values-at-risk can be overwhelming, especially in the face of uncertainty and randomness as well as the many types of alert levels. This paper is about sorting through risks and demands to make the best possible allocation of resources.

can be viewed as a "reinforcing/releasing" parameter for resource R based on resource r's demand data within HMZ G. It captures the propensity of current fire demand levels to influence the future fire suppression requesting. Since all HMZs share a pool of resources, we hypothesize demand in one zone may impact scarcity in another zone via common ODE feedback mechanisms. Adding r and g makes a more realistic model for how demand might follow risk and feedbacks on prior demand.

To regress our model onto data, we used finite difference methods in Matrix Laboratory (MATLAB). Given $n = 1, \ldots, N$ sample times t_n we computed maximum likelihood estimates of $a_{i,R,\,G,\,g}(t-s)$ for risks, $y_{R,r,\,G}(t-s)$ for release/reinforce, and $z_{R,G,\,g}(t-s)$ for sharing. Fitting the ODE model required us to assemble and organize numerical coefficient weight data into regression matrices $\boldsymbol{A}_{R,G}$ that capture the geometry of Eq. (1) . The regression data vector is comprised of fire demand change data $\overrightarrow{\partial_t U_{R,G}}$. The inverse problem of the ODE system is to fit the rate and level data at the sample times t_n with optimal numerical values for the vector of unknown parameters $\overrightarrow{x_{R,G}} = [\ a^s_{i,R,G,g}, y^s_{R,r,G}, z^s_{R,G,g}\ ]$. We solve sub-problems $\boldsymbol{A}_{R,G}\ \overrightarrow{x_{R,G}} = \overrightarrow{\partial_t U_{R,G}}$ by resource R and HMZ G. Since the resulting normal matrices $\boldsymbol{A}^T_{R,G}\boldsymbol{A}_{R,G}$ are nearly singular, we use conjugate gradient least squares [14] to invert and declare an optimum $\hat{x}_{R,G} \approx \boldsymbol{A}^{-1}_{R,G}\overrightarrow{\partial_t U_{R,G}}$ within numerical precision. Any *hât* above a parameter means a numerical approximation. We used MATLAB to assemble, parse, and analyze the inverse problem for this ODE system.

In summary, we formulated a system of $\#R \times \#G$ equations like Eq. (1) to denote a discrete time update in demand for resources in a multi-region hazard management system. In this way, each $ODE(R, G)$ equation like a moving average process. We fit a model for request rates and highlighted three sub-models. First, risk information is processed with a lagged memory. Second, sharing patterns among HMZs can have a self-reinforcing or self-depleting impact on demand across resources. Third, specific interregional sharing trends may change the rate update for any given HMZ. We interpret the coefficients as in any linear rate model:

$$\frac{dU}{dt} \propto \text{ fire risk } + \text{ reinforce/release } + \text{ sharing},$$

then solve the inverse problem to estimate all parameters. Since Eq. (1) is a linear constant coefficient inhomogeneous system of the form $U' = S\,U + f(a, D_i)$ we can comment on the stiffness ratio of S, in addition to providing a statistical fit for $f(a, D_i)$.

2.2. Incorporating geographic information system (GIS) data

Next, we explain how we calculated numerical estimates $\hat{x}_{R,G}$ to Eq. (1). There are many approaches to aggregate GIS data by HMZ. We chose to populate the matrix system $\boldsymbol{A}_{R,G}\ \overrightarrow{x_{R,G}} = \overrightarrow{\partial_t U_{R,G}}$ via a smoothed quadrature procedure. Discrete input data were smoothed with the radial basis function described in [15] according to fixed half-width radius $\kappa > 0$, before passing to the quadrature. Smoothing helped bias the model towards regional hotspots where concurrent natural hazard management has high demand for resources, but also be sensitive to small disparate hazard events in demand calculations.

Smoothed risk input data are re-gridded onto a common rectangular grid. Ignoring the elevation and curvature of Earth's surface, define spatial ordinates lx for ° longitude and ly for ∘ *latitude*. For example, (lx, ly) might be uniformly spaced $\Delta lx = \Delta ly$ in the $NAD83$ cartographic projection. Our specific procedure to calculate numerical risk weight data $D^s_{i,g}$ for each HMZ in Eq. (1) from GIS data $D_i(t-s, lx, ly)$ was as follows:

☐ Apply quadrature averaging rule via approximate integration

$$\overline{\overline{D^s_{i,g}}}(t) = \iint_{(lx,ly)\in\Omega_g} D_i(t-s, lx, ly)\ dlx\ dly \approx \sum_{\xi=1}^{M_\xi}\sum_{\eta=1}^{M_\eta} D_i(t-s,\xi,\eta)\ \Delta lx(\xi,\eta)\ \Delta ly(\xi,\eta) \tag{2}$$

Eq. (2) assigns a generalized "power" level associated with risk information layer i within HMZ g, at lag s. Eq. (2) permits unevenly spaced M_ξ-by-M_η grids where the grid widths are $\Delta lx(\xi, \eta)$ and $\Delta ly(\xi, \eta)$.

☐ Non-dimensionalization was performed on each risk information layer i independently. First, we scaled each quadrature estimate from Eq. (2) by the area of the HMZ

$$\overline{D^s_{i,g}}(t) = \frac{\overline{\overline{D^s_{i,g}}}(t)}{Area(\Omega_g)}, \tag{3}$$

Then, we re-scaled to [0, 1] based on the extreme values across the sample and lag points:

$$D^s_{i,g}(t) = \left(\overline{D^s_{i,g}}(t) - \min_{i,g,s}\overline{D^s_{i,g}}(t)\right) \Big/ \left(\max \overline{D^s_{i,g}}(t) - \min_{i,g,s}\overline{D^s_{i,g}}(t)\right) \tag{4}$$

Eqs. (2)–(4) show how to compute for any $t \in [T_0, T_F]$, $\overline{\overline{D^s_{(i,g)}}}(t) \to \overline{D^s_{(i,g)}}(t) \to D^s_{(i,g)}(t)$. These data are input to a system of ODE equations like Eq. (1); $U^s_{r,g}(t)$ was computed from the smoothed demand maps in the same manner. Thus, all demand data and risk information layers had equal numerical footing as input to the ODE system with components Eq. (1). As GIS data resolutions are typically much finer than the HMZ-level, many other options are available for performing this aggregation that would be application specific. Additionally, the following data transformations:

- Marginal first differences: $\partial_t D_i(t-s, lx, ly) = D_i(t-s, lx, ly) - D_i(t-s-\Delta t, lx, ly)$,
- Natural logarithm: $\log D_i(t-s, lx, ly)$, and
- Point-wise convolution: $D_i(t-s, lx, ly)^* D_{i'}(t-s, lx, ly)$ for $i \neq i'$

were used to form additional application specific candidate risk layers. These transformations permit the list of viable factors to be as rich and diverse as the problem requires.

2.3. Data sampling and solution method

Specifying the ODE inversion problem size was key to understand low rank conditions in the regression. Each best-fit $ODE(R, G)$ in Eq. (1) required the estimation of $|Lag(R,G)|(\#G(1+|FACTORS|) + \#R)$ parameters from N equations, where $|\cdot|$ gives the size of the sets. Data weights for the large number of parameters were assembled into each row of $\boldsymbol{A}_{R,G}$, while the small number of equations represents limited sample data or a lesser number of rows than columns in $\boldsymbol{A}_{R,G}$. The row dimension comes from including $|Lag(R,G)| * \#R$ reinforce/release demand coefficients $\hat{y}^s_{R,r,G}$, $|Lag(R,G)| * |FACTORS| * \#G$ risk coefficients $\hat{a}^s_{i,R,G,g}$, and $|Lag(R,G)| * \#R$ sharing coefficients $\hat{z}^s_{R,G,g}$. To make the numerical estimates, we inverted low rank matrices with column dimension $O(10^2)$ unknowns and row space dimension $O(10)$ equations. This underdetermined system was sensitive to noisy data inputs so we chose an *i.i.d.* sampling and replication method to resolve the parameter space in E numerical experiments. Each experiment fit a sample of N time moments $t_1, \ldots, t_N$ drawn at random with replacement from the archive. Sampling can be consecutive or nonconsecutive across the duration of the natural hazard.

During preliminary analysis, we found national Preparedness Level $PL = 1, 2, 3, 4,$ and 5 was significant to all ordinary least squares models. To enrich the study, we elected to use national PL to partition *apriori* the six years of 2011–2016 archive data into the 151 high alert days with $PL = 4$ *or* 5; and 405 normal status days with $PL = 2$ *or* 3.

By replicating these fits some number E times we were able to assess the range, variability, and significance of the true ODE system coefficients. Our test case descriptions mention the system and sampling sizes as $\langle \#R, \#G, N, E\rangle$. We wrote MATLAB code to assemble block structured matrices $A_{R,G}$ and calculate the best-fit regression coefficients, Appendix A explains this technique in more detail.

We found ordinary least squares estimates $\hat{x}_{R,G} \approx (\boldsymbol{A}_{R,G}^T\, \boldsymbol{A}_{R,G})^{-1}\boldsymbol{A}_{R,G}^T\,\overrightarrow{\partial_t U_{R,G}}$ required inversion of ill-conditioned regression matrices $\boldsymbol{A}_{R,G}^T\, \boldsymbol{A}_{R,G}$. To invert and solve under these low $rank(\boldsymbol{A}_{R,G}) = N$ and large $cond(\boldsymbol{A}_{R,G}^T\, \boldsymbol{A}_{R,G}) = O(10^{97})$, in the worst cases, we used two redundant inversion methods: iterative CGLS [14] and MATLAB's bicgstab.m. CGLS is a gradient-following algorithm to minimize regression residuals in the least squares sense. In this way, our numerical estimates in vector $\hat{x}_{R,G}$ are known to be a maximum likelihood estimates for the parameters given data $\boldsymbol{A}_{R,G}$ and $\overrightarrow{\partial_t U_{R,G}}$.

In using CGLS we are guaranteed local optimality to numerical precision of the computer because the final iterate will satisfy a first order necessary condition. The bicgstab.m algorithm does the same. Redundancy in matrix inversion method ensured a consistent model-fit because bicgstab.m converged within numerical tolerance to the CGLS estimates. We do not have any guarantee of global optimality via second order conditions, but the replication of coefficient fit helped us characterize weakly global minimum residuals.

2.4. Test cases, U.S. data – 2011 through 2016

Our test cases include the contiguous United States, Alaska, and Hawaii from 2011 to 2016. We compiled historical databases for fire suppression demand by resource as well as fire risk information layers. The resolution of our database was $\Delta t = 1$ *day* and $0.08^\circ \le \Delta lx,\ \Delta ly \le 0.16^\circ$, the approximate degree equivalents of 9 km and 18 km grid spacing. We selected four types of terrestrial resources and three aerial types to build our test cases (Table 1). The United States have large HMZs organized into Geographic Area Coordination Centers. Our interregional sharing test cases involve these regions (Table 2). Our statistics show which of the viable factors in Table 3 as well as derived and combined factors in Table 4 apply to which resources on a national scale as well as between regions. Since fire suppression work is seasonal, time-limited by a soft 14-day and firm 21-day work limitation rule (Preparedness Levels, National Interagency Mobilization Guide, Chapter 20), and pulsed [16], we also analyzed periodicity by fitting lagged data.

Eq. (1) was localized to the United States as a national sharing model with $\#G = 12$. Eqs. (2)–(4) implement a coarse spatial aggregation, which we assemble into the matrix $\boldsymbol{A}_{R,G}$, then solve as an inverse. This procedure carries the assumption that each region consists of similar decision-makers. We used it to find any patterns in how these groups detect risk and generate fire demand. We designed the following three test cases to better understand how the model in Eq. (1) may or may not describe trends in fire demand:

- **(ALL)** *The full ODE system was tested in all-regions*. Sampling results across a set of single, derived, and combined GIS layers for $|FACTORS| = 45$ are available in Tables 3 and 4. Interested readers can see Appendix B for more information about computation and storage limitations of the new ODE method, but this large problem $\langle \#R = 7, \#G = 12, N = 16,\ E = 17\rangle$ was tractable to solve by most computers.
- ***(Regional Analysis)*** Two smaller test cases with $\langle \#R = 4, \#G = 2, N = 10, E = 23\rangle$:
- **(Rockies)** This was a risk sensitivity analysis of fire demand within the Rocky Mountain Area Coordination Center RMCC and the Southwestern Coordination Center SWCC. These HMZs cooperate perennially because the monsoon weather patterns support spring and early summer fire in the SWCC, while the RMCC heats up in middle and late summer.
- **(California)** A parallel analysis between the Northern Operations Coordination Center NOCC and the Southern Operations Coordination Center SOCC, which are the regional HMZs for northern and southern California. California orders from ROSS, but share a substantial pool of state-level resources. It is a region that will continue to have high workloads in the future.

Test cases **(Rockies)** and **(California)** have $\#G = 2$ adjacent regions from Table 2 and the $\#R = 4$ terrestrial resources from Table 1. These neighbor-to-neighbor collaborations were of interest to study and the associated ODE system has eight ODEs like (1). Table 5 gives an example of three of these eight ODEs explaining key overlaps by resource and by region as well as reiterating the terms: sharing, risk, and reinforce/release.

We solved an inverse problem for the ODE system by simultaneously inverting each member equation of Eq. (1). We indexed and displayed our results by lag $s \in \{0, 1, 2, 3, 7, 14, 21\}$, suppression resources R, regions G, and risk information $i \in FACTORS$. We analyzed significance, variability, and mean tendency of the best-fit coefficients to the ODE system in using the N-sample, E-replicate procedure outlined in the methods section. We assumed each parameter to be normally distributed. We determine the significance of each estimate at a 95% confidence level finding p-values at $\chi^2_{E-1,0.05}$.

Table 5
ODE equation coupling $(R, G) = (3, 2);\ (3, 3);\ (4, 3)$.
In producing the ODE system with building in Eq. (1), the model detects if the RMCC and SWCC respond differently to the same fire demand. We assume that the RMCC managers might account for ordering and resource use in the SWCC and visa-versa. In the (top-left boxes), engines use identical demand data $U_{3,2}(t-s)$ and fit different coefficients $\hat{z}^s_{3,2,2}$ and $\hat{z}_{3,2,3}$. In the bottom-right box, the SWCC uses identical demand data, but allows for a cooperative effect.

	Sharing	Risk	Reinforce/release
$\vdots$			
Engine, RMCC $\frac{dU_{3,2}}{dt}(t) =$	$\hat{z}^s_{3,2,2}\, U_{3,2}(t-s) + \hat{z}^s_{3,2,3}\, U_{3,3}(t-s)$	$+ \sum_{i=1}^{L} \left(\hat{a}^s_{i,3,2,2}\, D_{i,2}(t-s) + \hat{a}^s_{i,3,2,3}\, D_{i,3}(t-s)\right)$	$+ \hat{y}^s_{3,1,2}\, U_{1,2}(t-s) + \hat{y}^s_{3,2,2}\, U_{2,2}(t-s) + \hat{y}^s_{3,3,2}\, U_{3,2}(t-s) + \hat{y}^s_{3,4,2}\, U_{4,2}(t-s)$
Engine, SWCC $\frac{dU_{3,3}}{dt}(t) =$	$\hat{z}^s_{3,3,2}\, U_{3,2}(t-s) + \hat{z}^s_{3,3,3}\, U_{3,3}(t-s)$	$+ \sum_{i=1}^{L} \left(\hat{a}^s_{i,3,3,2}\, D_{i,2}(t-s) + \hat{a}^s_{i,3,3,3}\, D_{i,3}(t-s)\right)$	$+ \hat{y}^s_{3,1,3}\, U_{1,3}(t-s) + \hat{y}^s_{3,2,3}\, U_{2,3}(t-s) + \hat{y}^s_{3,3,3}\, U_{3,3}(t-s) + \hat{y}^s_{3,4,3}\, U_{4,3}(t-s)$
Dozer, SWCC $\frac{dU_{4,3}}{dt}(t) =$	$\hat{z}^s_{4,3,2}\, U_{4,2}(t-s) + \hat{z}^s_{4,3,3}\, U_{4,3}(t-s)$	$+ \sum_{i=1}^{L} \left(\hat{a}^s_{i,4,3,2}\, D_{i,2}(t-s) + \hat{a}^s_{i,4,3,3}\, D_{i,3}(t-s)\right)$	$+ \hat{y}^s_{4,1,3}\, U_{1,3}(t-s) + \hat{y}^s_{4,2,3}\, U_{2,3}(t-s) + \hat{y}^s_{4,3,3}\, U_{3,3}(t-s) + \hat{y}^s_{4,4,3}\, U_{4,3}(t-s)$
$\vdots$			

In using the ODE method, we provide statistical inference for the maximum likelihood of the parameters in $\overrightarrow{x_{R,G}}$ using samples in test cases **(ALL)** and **(*Regional Analysis*)**. While our test cases are localized to the United States, we have stated the model in general terms, so peoples from other countries can also adopt the method.

3. Results

3.1. Interregional resource assignment and factor data analysis

This section shows the results of test cases **(ALL)** and a wildfire hazard application summary for **(Rockies)** and **(California)**. This section refers to Tables 6 and 7 and Figs. 2–7. To obtain these results we assumed wildfire hazard demand for resources evolved according to the system in Eq. (1). The sampling and replication approach revealed which coefficients were the most significant ones to the interregional management from 2011 to 2016. In computing likelihood statistics for each parameter in the ODE model we revealed trends in fire suppression resource allocation that will be useful to hazard management practitioners setting regional response strategies.

Before describing the model results, Fig. 2 is an infographic about a single replicate for $N = 10$ sample days. These data were processed $\overline{\overline{D^s_{i,g}}}(t) \rightarrow \overline{D^s_{i,g}}(t) \rightarrow D^s_{i,g}(t)$ according to Eqs. (2)–(4). This plot demonstrates important features of the risk and demand data for which we seek best-fit ODE coefficients. One feature is collinearity among the large number of viable, derived and combined factors $D_i(t-s,\ lx,\ ly)$, an issue that required special numerical treatment.

Next, we report numerical estimates and bounds on the values of significant risk and demand coefficients in Eq. (1). All results from **(ALL)** and ***(Regional Analysis)*** are specific to the fire application area *and make substantial use of abbreviations in* Tables 1–4, but the analysis procedure would apply in other multi-region natural hazard resource management applications.

*3.2. Test case **(ALL)***

Table 6 shows which of the risk factors (all lags) in Table 3 were found to be significant for a few highlighted resources and regions. One advantage of Table 6 is to provide a quick answer to any “was risk factor i part of the best fit for resource R data in region G?” A general trend in these color-coded tables is a contrast between the explanatory variables identified from the high alert PL45 (top) fire days and the normal status PL23 (bottom) fire days. The list of significant risk variables used to predict regional resource demand tend to be much shorter for normal status fire days.

On normal status days, we typically found three or four significant $\hat{a}^s_{i,R,G,g}$ with $p < 0.01$ at the 95% level according to $\chi^2_{E-1,0.05}$. On high alert days there were between six and ten significant coefficients. This is an important verification because the PL45 category should have – per (National Interagency Mobilization Guide, Chapter 20) – significantly higher level of mobilization than PL23 normal status. Table 7 is a specific region/resource subset from Table 6 with additional information about the relative yearly workloads measured by the frequency of resource deployment. For instance, EGBCC and WGBCC dozer use, while less frequent than FFT2 use, seems to be explained by as many as eight factors, whereas it takes five or fewer to create the best fit for FFT2s. A practitioner might notice engine demand in the NOCC follows both large fires and

Table 6
Results of test case **(ALL)**, ODE fit model performance.

$PL45$	EACC	RMCC	SWCC	EGBCC	WGBCC	SACC	NWCC	NRCC	NOCC	SOCC
constant	--34 ---	--3- ---	1-3- 56-	---- ---	1--- 5-7	12-4 56-	1--- -67	--3- -67	123- 567	---- -6-
MODIS	1—4 5-7	---- --7	--3- 5-7	---4 -67	--34 -6-	-2-4 ---	123- ---	12-- -67	1--- 56-	---- ---
ERC	1--- ---	---- --7	1-3- 567	1234 5--	---4 --7	-2-- ---	1-3- 567	-234 56-	--3- -67	1--- ---
FOD	12-- --7	1--- ---	1--- 56-	-234 -67	12-4 -67	12-4 ---	--34 567	1-34 -6-	1--4 -67	12-- -6-
BI	1234 5-7	1-3- 5-7	---4 567	1234 -67	--34 -6-	12-4 ---	---4 ---	123- -67	123- -67	1--- ---
regionPL	1-3- 5--	-234 ---	--3- 56-	-2-- ---	---- 5--	-2-- ---	12-4 ---	---- 5-7	---- -6-	--3- --7
WindVel	123- ---	--34 5--	123- 567	1--- 567	1--4 -6-	12-- ---	123- ---	--3- --7	1234 ---	1--- -67
geDIST	--34 5--	--3- ---	--3- 5--	---- ---	1--4 --7	-2-- 56-	1--- ---	---- --7	---4 5--	1--- ---
log *LSNITE*	---- ---	---- 56-	--3- 56-	---- --7	---4 ---	-2-- ---	1--- ---	---4 --7	1--- ---	---- ---
COST	12-4 ---	123- ---	-2-- -67	---- 5-7	---4 -67	-2-4 -6-	1--- ---	--3- 5-7	---- 5--	---- -6-

$PL23$	EACC	RMCC	SWCC	EGBCC	WGBCC	SACC	NWCC	NRCC	NOCC	SOCC
constant	---4 ---	-2-- ---	---- --7	1--- -6-	---4 56-	12-4 ---	1--- 5--	---- 5--	12-4 567	---- ---
MODIS	---4 ---	123- ---	---- ---	---- -67	1234 56-	--3- -6-	123- -6-	12-- ---	1234 -6-	-2-- ---
ERC	---4 5--	-234 -6-	---4 -67	12-4 -6-	-2-- 56-	-2-- ---	12-- 56-	-2-- ---	12-4 567	---- --7
FOD	1--4 5--	---- -6-	---- --7	1-34 -6-	1234 5-7	--3- 5--	12-- 567	---4 ---	123- 567	--34 -67
BI	---4 ---	123- -6-	---- 5--	-2-- -67	-234 ---	1-34 5--	---- -6-	---4 ---	---4 ---	-23- -6-
regionPL	---4 ---	-23- ---	---- ---	-23- -67	--34 567	-2-4 -6-	-2-- 56-	---4 ---	12-4 -67	---- ---
WindVel	---4 5--	-2-4 -6-	1--- ---	1-34 -67	1-34 56-	---- ---	-2-4 -67	---- ---	1--- -6-	---- 5--
geDIST	-2-4 ---	12-- ---	---- ---	1-34 -67	--34 56-	12-4 -6-	---4 ---	1--- ---	12-- -6-	---4 5--
log *LSNITE*	---4 ---	123- ---	--3- ---	---- 56-	-2-- 56-	---- ---	---- ---	---- ---	12-- -6-	---- ---
COST	---4 5--	1-3- -6-	1--- ---	1-34 -6-	--34 567	---4 ---	-2-4 -6-	---- --7	-2-4 -6-	---- ---

Table 7
ODE best-fit results for selected resources and regions.

	*PL*45/*PL*23 **X** = $p < 0.01$ **–** = $p \geq 0.01$ *2011–2016* *# of assignments &* *reassignments per year* [median] max, min	`constant`	`MODIS`	`ERC`	`FOD`	`BI`	`regionPL`	`WindVel`	`geDIST (static)`	`log LSNITE (static)`	`COST`	*# of factors*
Dozers												
– EGBCC	[57] 393, 3	**–/–**	**X/–**	**X/X**	**X/X**	**X/–**	**–/–**	**–/X**	**–/X**	**–/–**	**–/X**	*4/5*
– WGBCC	[390] 1034, 66	**–/X**	**X/X**	**X/–**	**X/X**	**X/X**	**–/X**	**X/X**	**X/X**	**X/–**	**X/X**	*8/8*
FFT2s												
– EGBCC	[6366] 22,182, 397	**–/–**	**–/–**	**X/X**	**X/–**	**X/X**	**X/X**	**–/–**	**–/–**	**–/–**	**–/–**	*4/3*
– WGBCC	[8081] 15,102, 42	**–/–**	**–/X**	**–/X**	**X/X**	**–/X**	**–/–**	**–/–**	**–/–**	**–/X**	**–/–**	*1/5*
FFT1s												
– NOCC	[18,405] 26,965, 2910	**X/X**	**X/X**	**–/X**	**X/X**	**X/–**	**–/X**	**X/X**	**–/X**	**X/X**	**–/–**	*6/8*
– SOCC	[23,431] 46,199, 7251	**–/–**	**–/–**	**X/–**	**X/–**	**X/–**	**–/–**	**X/–**	**X/–**	**–/–**	**–/–**	*5/0*
Engines												
– NOCC	[20,115] 31,616, 3051	**X/–**	**–/X**	**X/–**	**–/X**	**X/–**	**–/–**	**X/–**	**–/–**	**–/–**	**–/–**	*4/2*
– SOCC	[14,679] 42,249, 7827	**–/–**	**–/–**	**–/–**	**–/X**	**–/X**	**X/–**	**–/–**	**–/–**	**–/–**	**–/–**	*1/2*
– RMCC	[3992] 17,629, 971	**X/–**	**–/X**	**–/X**	**–/–**	**X/X**	**X/X**	**X/X**	**X/–**	**X/–**	**–/X**	*6/6*
– SWCC	[72,985] 22,893, 2740	**X/–**	**X/–**	**X/–**	**–/–**	**–/–**	**X/–**	**X/–**	**X/–**	**X/X**	**–/–**	*7/1*

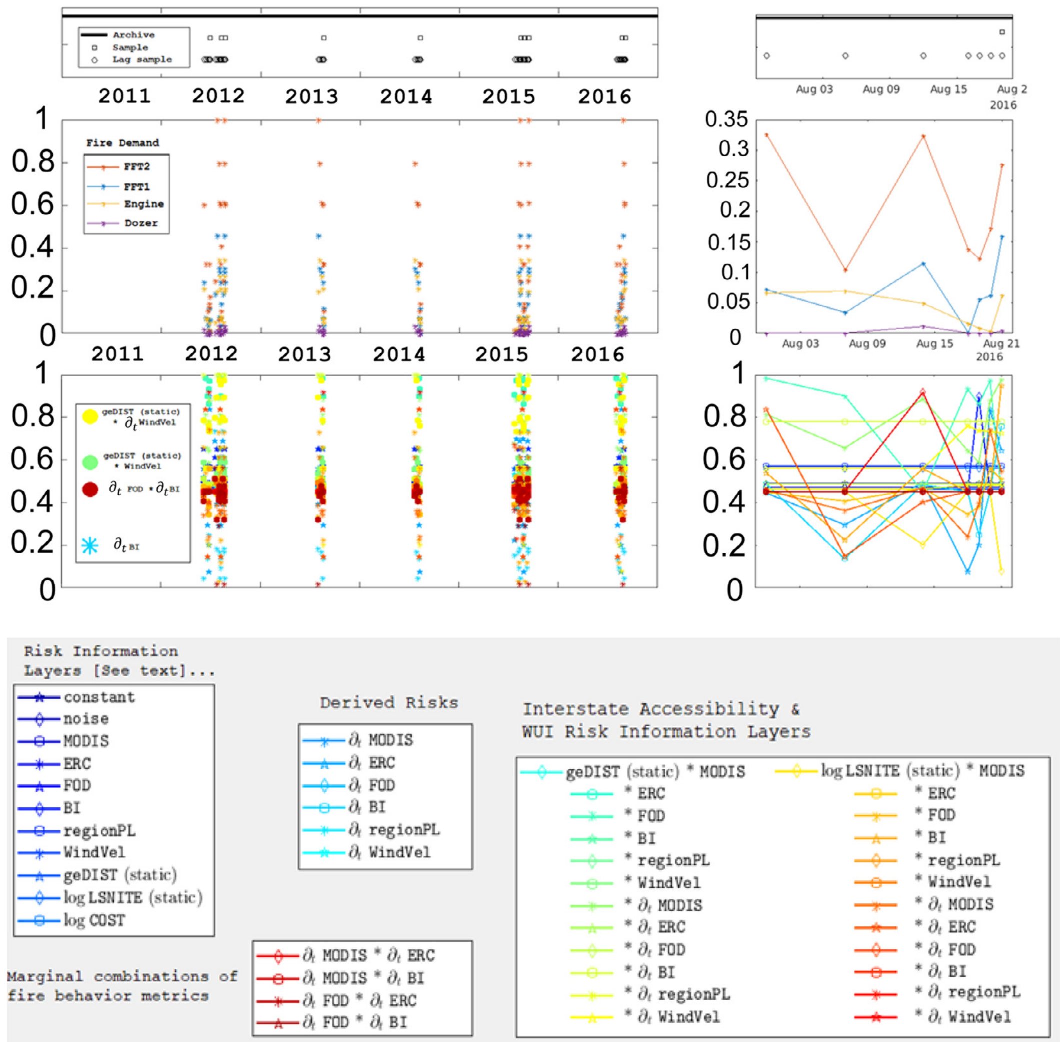

Fig. 2. ODE method input data sample.
[Left panel] (Top plot) *N*-day, *E*-replicate time sample structure. (Middle plot) central tendency of risk data in sample is near 0.5. (Bottom plot) some input statistics from which the visual estimate of mean μ and variance σ^2: $geDIST\,(static)^{*}\partial_t WindVel\,(t-s) \sim \mathbf{N}(\mu=0.80,\ \sigma^2 < 0.14)$; $geDIST\,(static)^{*}WindVel\,(t-s) \sim \mathbf{N}(\mu=0.59,\ \sigma^2 < 0.14)$; $\partial_t FOD^{*}\partial_t BI\,(t-s) \sim N(\mu=0.47,\ \sigma^2 < 0.01)$; and lastly any recent changes in Burning Index $\partial_t BI(t-s) \sim N(\mu=0.25,\ \sigma^2 < 0.14)$
[Right panel] (Top plot) lag structure within each sample. (Middle plot) a correlated surge of demand for firefighters on August 15th, a period of lower demand, followed by a spike in fire demand coinciding with the August 21st sample. (Bottom plot) bundles of lines move together, multicollinearity in inputs.

general ignition detections at normal status, but pegged to fuel condition variables, winds, and a constant at high alert. Also, ongoing expenditures were rarely among the best-fit parameters in Table 7. It hints that cost is not a strongly expressed risk preference in ROSS ordering lists. Some disadvantages of Tables 6 and 7 are they mask the relative weights, confidence intervals, and any lag information.

Fig. 3 shows how the lag sum in Eq. (1) is used in a model for risk processing. Predicting tomorrow's demand in fire hazard management may depend on prior events up to three weeks ago. The plots in Fig. 3 have large bands of uncertainty, but certain coefficients can be reported as significantly positive or negative. In terms of a hazard management model, the ODE system general results have been important to validate the model for wildfire data. Figs. 1–3 have explained the progression from GIS data to normalized regional averages to specific observations and recommendations for the application area risk and demand 2011–2016 database. This analysis could indeed be performed with flood risk factors, storm characteristics, and climate data to support ODE analysis of another type of natural hazard. We will now focus on what can be learned from the ODE with the goal of improving hazard response for wildfire.

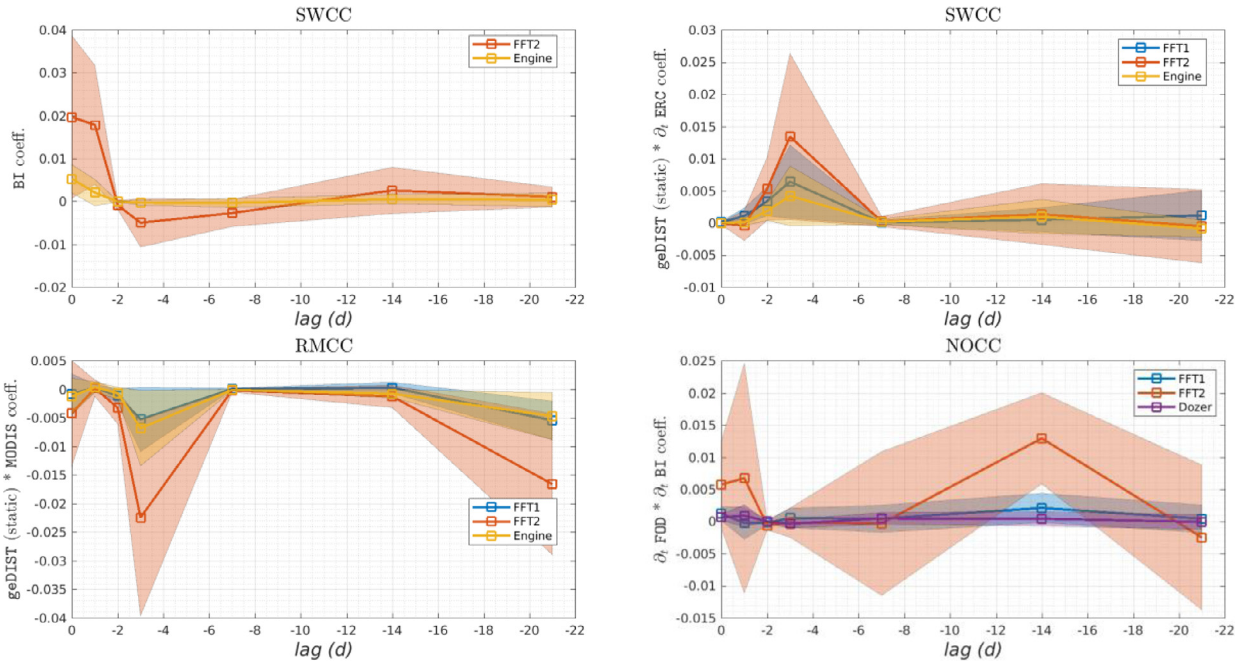

Fig. 3. Significance of lagged information.
Four significant lag coefficients are shown. Past information matters when setting demand for wildfire hazard resources. (Top left) Short term – 0 to −3 days – lag prevalance for *BI* when fit to FFT2s and engines on the SWCC because *BI* is a measure of fuel combustability, which manifest as additional fire growth and more resource use. (Top right) Again in the SWCC, a spike in the accessibility convolved with changing dryness indicates resource needs may follow remote drying exactly three days later. (Bottom left) Negative values in the RMCC mean demobilization trends up to a 21-day lag. (Bottom right) In NOCC, there seems to be a coordination among FFT2s near the 14-day rotation limit that is stronger than FFT1s and dozers.

3.3. Test case (Rockies)

In test case **(Rockies)**, we studied the demand of four resource types {FFT1, FFT2, engine, dozer} in two regions {RMCC, SWCC}. We found large fire detection information like $MODIS(t-s)$ and fire control difficulty indicator such as $BI(t-s)$, and other risk factors derived from them have strong $p < 0.01$ significance for FFT1s and engines. This confirms current research and thinking about the focal roles of these resources in the suppression of large fires. Fig. 4 shows three panels – a, b, and c – of strongly $p < 0.01$ and weakly $p \in [0.01, 0.045]$ significant coefficients. This style of influx and outflux plot was useful for understanding wildfire hazard demand and risk data; the circle/star marker pairs indicate whether the demand was related to internal (self) information or the risks in the companion region. Fig. 4(a) shows FFT1 in the SWCC demobilization trends are described by a larger number of significant coefficients than mobilization trends on normal status days. While not true in every model we fit, we found in general: inflow of resources into a region is more predictable from risk information than outflow out of a region under the ODE model. In the case of wildfire suppression and its 14-day shift length, as a fire gets contained and dies down, demobilization happens gradually and is less predictable from the list of viable factors that the initial hazard.

Fig. 4(b) shows the best-fit risk coefficients for engines in the RMCC. Comparing FFT1 in the SWCC to engines in the RMCC reveals – on normal status PL23 days – it was common for large fire incidents. Interestingly, the coefficient on $\partial_t ERC(t-14)$ was positive and as significant to the demand data as some of the large fire indicators. In the ODE style model, this proportionality: $\frac{\partial U}{\partial t} \propto \partial_t ERC(t-14)$ is easy to interpret. Areas that were drying out at the start of the last shift demand resources this shift. Fig. 4(c) shows engines in the RMCC when the national alert climbs to PL45. The same coefficients are still significant, but the lag structure is not evident and other, confounding factors have entered the best-fit model. A 14-day lag in this case does not make sense because it is quite restrictive for high alert days, thus, the absence of significant lagged variables confirms out intuition. We are not sure why so many more factors appear significant when the sharing system is stressed. Finally, RMCC engine demand model demonstrates an instance of high alert samples having more significant explanatory variables than normal status days – there were 25 as opposed to 14.

To demonstrate what this model might reveal about policy, we make an additional observation about Fig. 4(c). Notice there is no delay (lag) for the RMCC to order more resources at high alert PL45 level, if they discover high BI and MODIS. There is, however, a 7-day delay for the RMCC to order more resources due to the increase of fire activity at PL45. This model suggests the RMCC might pay more careful attention to escalating of fire activities with a slightly longer memory. Today's severe fire behavior and last week's both inform demand.

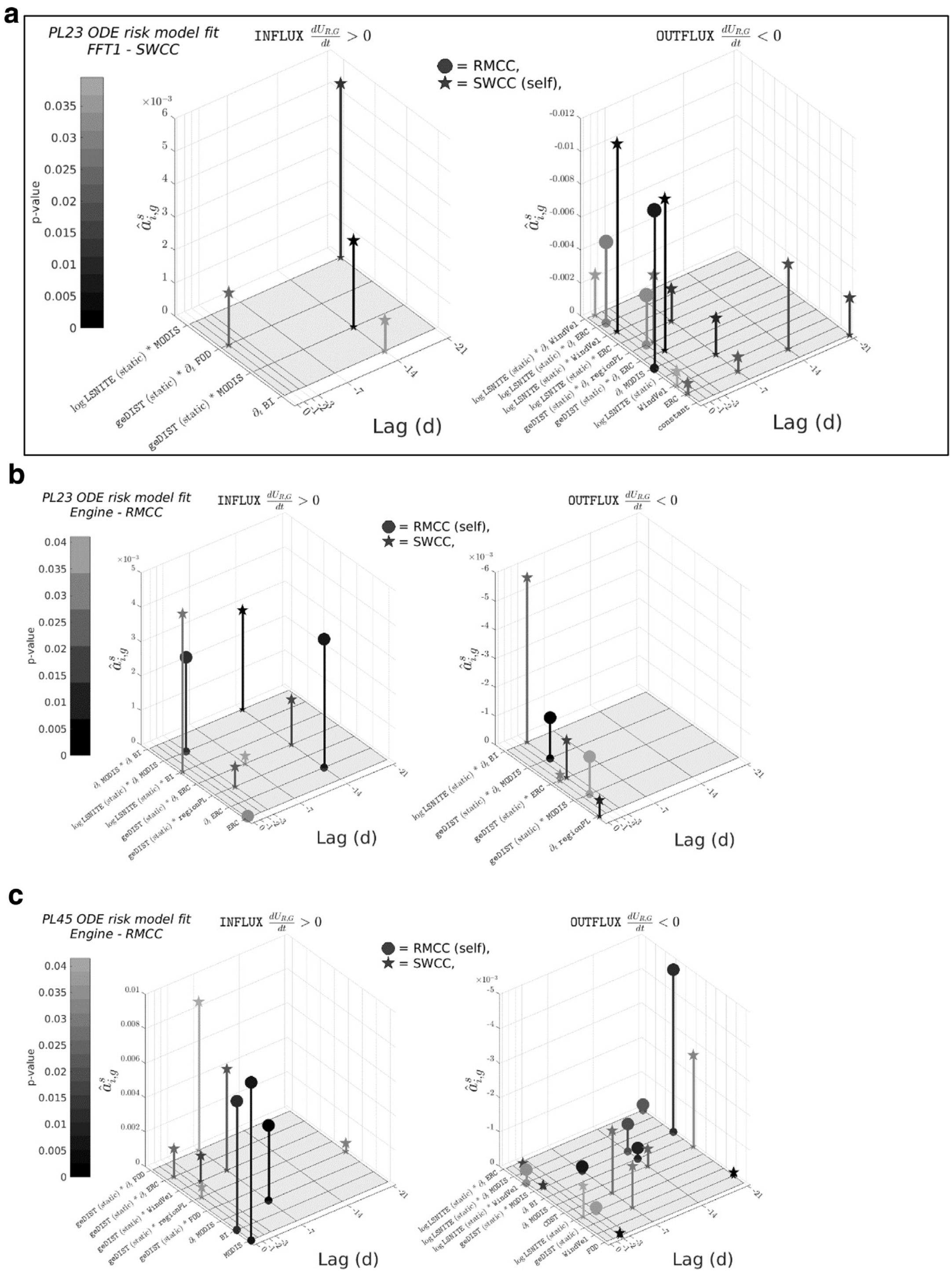

Fig. 4. FFT1s and engines test case **(Rockies)**, best fit ODE risk sub-model.
Throughout notice *MobETA* is on the left panel and *MobETD* is on the right panel. (a) Foreground axes are for *Lag* and *FACTORS*. Vertical axes are for the coefficient's mean value over *E* replicates. The left plot shows mobilization to incidents in the region. The right plot has its axes reversed to display release or demobilization from incidents in the region. Dots and markers specify the coefficient belongs to the same (self) or the other in these two-region sharing models. A bar at the left gives the significance of the coefficient within our two ranges $p < 0.01$ and $p \in (0.01, 0.0435]$. Each plot set is specific to the high alert versus normal status sample, resource, and region in the ODE model being fit i.e. in the above instance *PL*23 sample results for FFT1 in the RMCC. Our analysis for (b) and (c) is in Section 3.3.

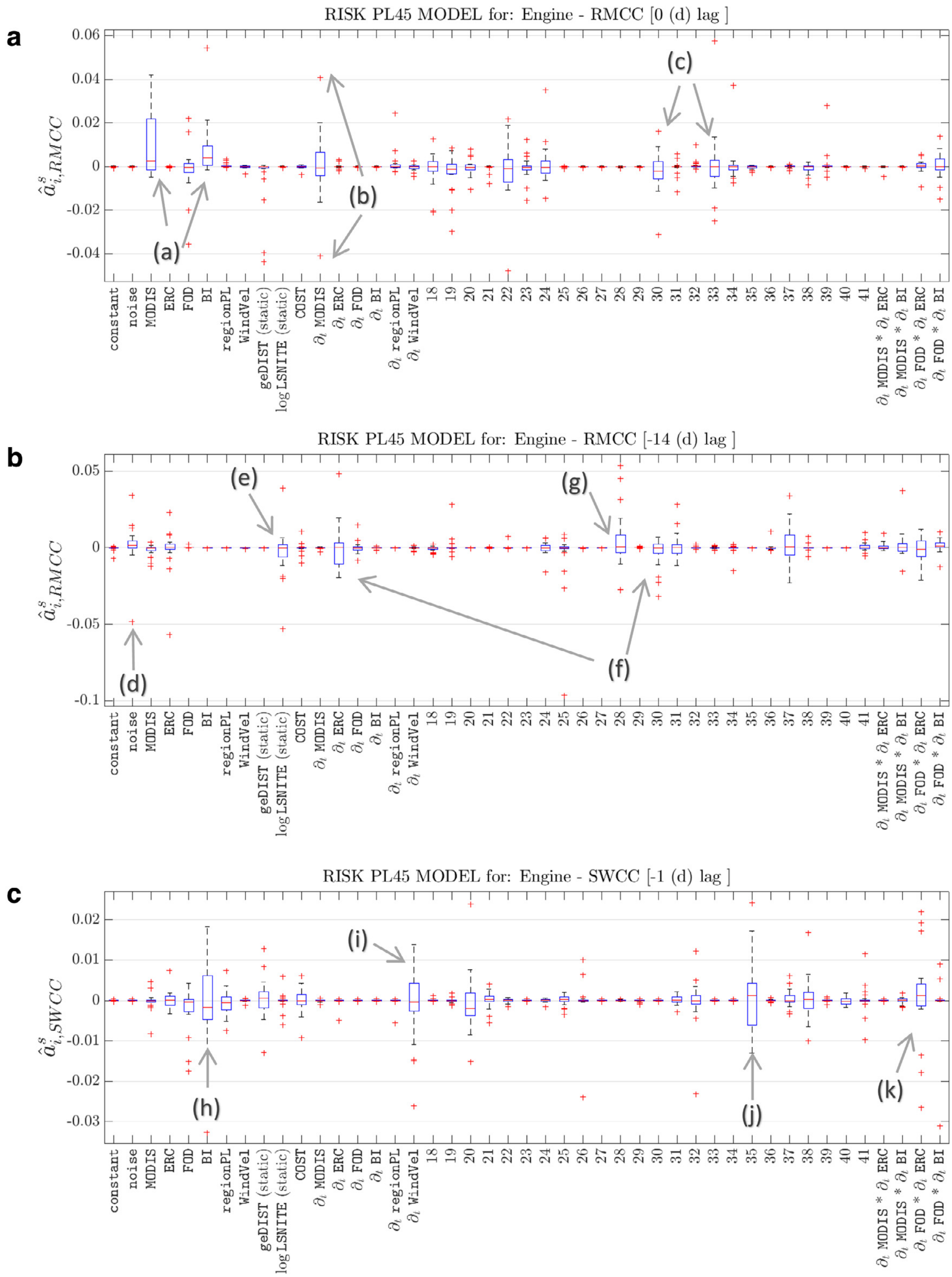

Fig. 5. Engines test case (**Rockies**), variability of ODE model coefficients.
Best fit engine ODE models. All GIS layer fit display, all *FACTORS* shown. Vertical box-and-whisker plots across *E* replicates for best fit risk coefficients to the $N = 10$ sample days from the PL45 archive. Subtitles indicate for which resource, region, and lag the inversion results apply. Comments (a)–(k) in Section 3.3 explain how we interpret the variability and outliers.

Fig. 5 shows all coefficients, even ones that are not significant or show mean tendency near zero. These plots show variability of risk coefficients across-samples and reveal fit outliers but cannot indicate significance.

We have highlighted the following observations for lag $s = 0$ coefficients in Fig. 5(a):

(a) Today's large fire behavior metrics measured by $MODIS(t)$ and $BI(t)$ drive engine ordering in the RMCC.
(b) Similarly, outliers in the $\partial_t MODIS(t)$ coefficients at the $\pm$ 0.04 level indicate changes in large fire activity can precipitate substantial mobilization and demobilization of engines in the RMCC.
(c) Moreover, engine mobilization in the RMCC is conditioned on severe fires near the WUI because combined layers $\log LSNITE{*}MODIS(t)$ and $\log LSNITE{*}BI(t)$ have variable signals. See Table 4 for more information about combined layers and the WUI metric $\log LSNITE$ used in our study.

Both large fire metrics and *ERC* at a 14-day lag also play a role in engine management in the RMCC. We highlighted some more observations for lag $s = 14$ coefficients in Fig. 5(b):

(d) $p < 0.01$ When noise$(t - 14)$ is significant it means none of the other risk information layers successfully explain the mobilization of engines in the RMCC.
(e) Resource release according to the 14-day limit from fires near the WUI might supersede other risks in requesting for new suppression resources.
(f) Seasonal drying of fuels reflected by ERC$(t - 14)$, ∂_tERC$(t - 14)$, and combined log LSNITE data drive engine allocation in the RMCC.
(g) Changes in regional alert levels seem to matter most when combined with the accessibility of an incident through interstate highways.

Engine mobilization in the SWCC exhibits similar 0- and 14-day patterns with $MODIS(t)$ and $BI(t)$ driving the process, especially on WUI fires. Fig. 5(c) looks at 1-day lag patterns for engines in the SWCC. Wind and detection of new fire starts have higher variability than those for 1-day large fire indicators. We have highlighted the following observations in Fig. 5(c):

(h) BI$(t - 1)$ has a strong signal likely due to large fires to produce ordering the day after a spike in fuel flammability.
(i) Our ∂_tWindVel$(t - 1)$ layer captures a change in wind direction and shows strong signal in the best-fit engine model for the SWCC; changing winds often correspond to increased fire activity as the heat might be steered towards new beds of unburned fuels.
(j) High winds speeds near the WUI have a strong signal for the engine SWCC model because of the threat posed to structures under these conditions.
(k) Many layers include yesterday's fire starts FOD$(t - 1)$, but this hybrid metric of ∂_tFOD$^*\partial_t$ERC$(t - 1)$ is particularly interesting because it supports rapid changes in fuel moisture as a critical factor for fire starts.

The same trends (a)–(k) are present in the FFT1 results. Furthermore, FFT1 coefficients in the SWCC share the characteristic 1-day lag switch from large fire response, to anticipating large fire using wind and fire starts.

3.4. Impacts of demand

As one might expect, each resource *R* in the ODE fire management model can have an entirely different coefficient of proportionality for $\frac{\partial U_{R,G}}{\partial t} \propto U_{R,G}$ and those dependencies may vary by region *G*. We found the ODE assumptions for the demand model in Eq. (1) only seem to apply for engine coordination in the four study regions {RMCC, SWCC, NOCC, SOCC}. In this case, the ODE model may serve as a suggestion of how coordination might be managed in the future. The next paragraph transmits our findings.

All demand coefficients exhibit a common time signature. It applies to both the reinforce/release demand in $\hat{y}^s_{R,r,G}$ and the sharing impact of demand in $\hat{z}^s_{R,G,g}$. In terms of the sharing coefficients, we found a central tendency for $\hat{z}^0_{R,G,g} > 0$ meaning today's orders are filled tomorrow in rate data $\frac{dU}{dt}$ for {FFT1, FFT2, engine, dozer}. For lag $s = 1$ we found $\hat{z}^{-1}_{R,G,g} < 0$ indicating it is rare to order the same resource to the same region two consecutive days in a row. By assembling the significant reinforce/release coefficients into sub-matrix *S*, we computed a stiffness ratio of $\bar{S}_{Rockies} = 0.0014$ for the resource and region sharing. This is comparatively smaller to the stiffness ratio $\bar{S}_{California} = 27.3847$, which we computed from the following test case.

3.5. Test case (California), intercomparison ODE model

We report test case **(California)** in order to compare and contrast {FFT1, FFT2, engine, dozer} use in {NOCC, SOCC} with their use in {RMCC, SWCC}. For demand impacts, we found internal coordination within California is stronger than within the central/southern Rockies. Many of the significant reinforce/release parameters suggest California coordinates FFT1 allocation in the short-term and FFT2 allocation in the long-term.

Fig. 6 echoes Fig. 4 showing the best-fit risk models for FFT1s in the SOCC during normal status fire days, engines in the NOCC at during normal status fire days, and engines in the NOCC during high alert fire days. Both pairs of adjacent regions change their sharing practices according to the national PL, with high alert fire days resulting in noisier ODE output models.

Key differences in the best-fit ODE models between **(Rockies)** and **(California)** are shown in Fig. 6:

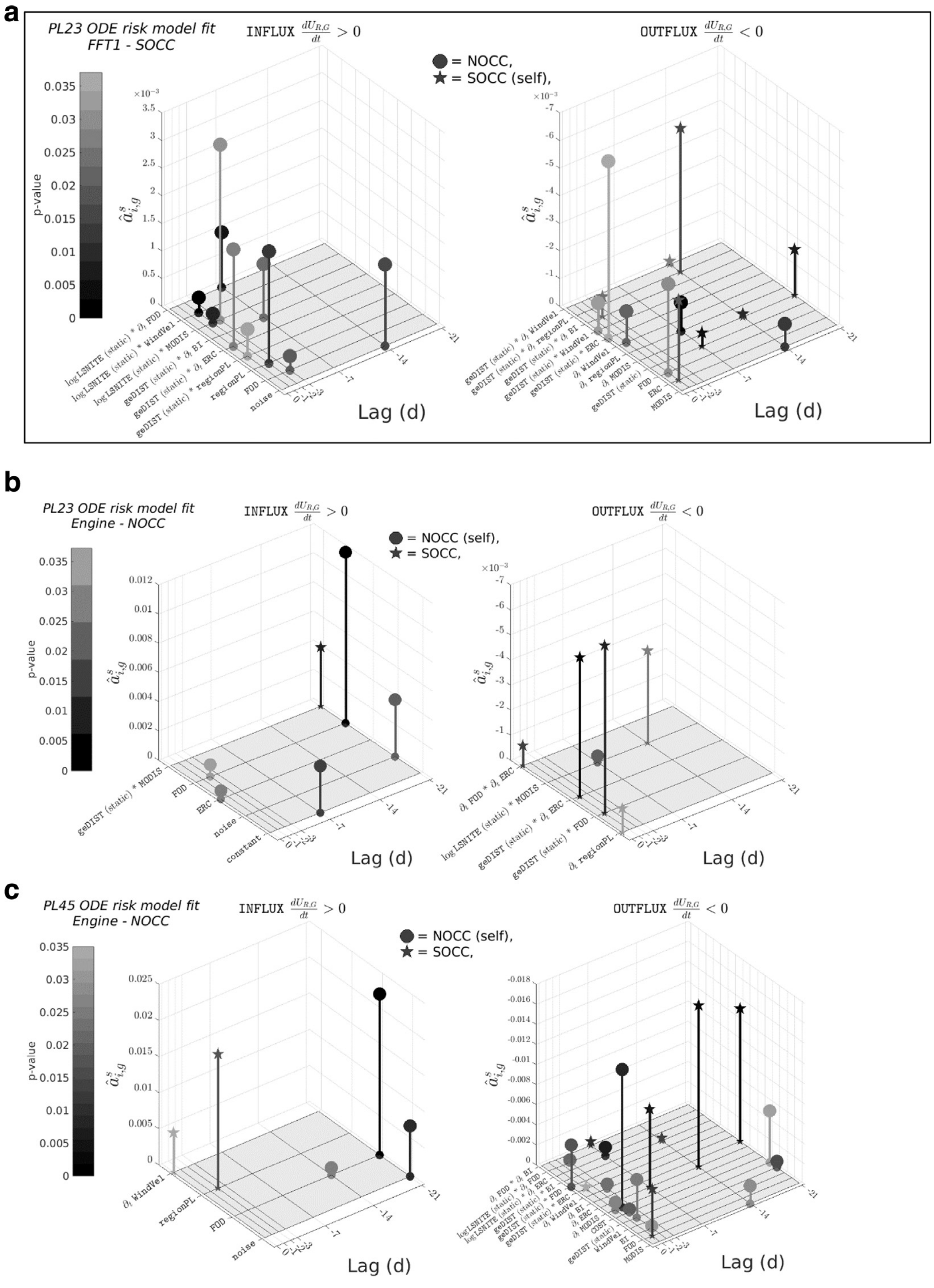

Fig. 6. FFT1s and engines test case **(California)**, best fit ODE risk sub-model.
California risk results for test case **(California)**. Compare with Fig. 4. Again, notice *MobETA* is on the [LEFT PANEL] and *MobETD* is on the [RIGHT PANEL]. (a) shows the 14-day lag is only prevalent *noise*$(t-14)$, focus on 2- to 7-day risk response. FFT1s have ten coefficients mobilization model in the SWCC as compared with four in the SOCC. (b) California has different risk models than the central/southern Rockies. Closer coordination is evident in demobilization for {NOCC, SOCC} as compared with {RMCC, SWCC}. (c) Large fire data focus in the RMCC, but not so in the NOCC.

– California is less influenced by lagged information, but rather 2- to 7-day risk responses.
– FFT1s have a much sparser mobilization model in the SWCC with fewer numbers of significant risk variables as compared with the SOCC.
– Elevated risk is associated with significant coefficients on large fire data in the RMCC, but not so in the NOCC.

Additional comparisons between the risk factor charts in Figs. 4 and 6 might help practitioners evaluate the best GIS risk layers to use by resource and by region. The purpose of considering small interregional comparison models is to demonstrate how the ODE method is used on a regional scale. As north/south neighbors we might expect that NOCC and SOCC may face similar challenges to wildland firefighting allocation on multiple fires as the RMCC and SWCC. However, California tends toward tighter fire suppression focused on quick response, whereas the Rockies shows some shift-length rotational trends.

4. Discussion

Our system of ODEs was developed to reveal when and where spatiotemporal correlation occurs in allocation data for natural hazard management resources and was applied to wildland fire suppression data. Our best-fit models differentiate between mobilization and demobilization of wildland suppression resources. We used three test cases to verify the model detects known allocation patterns, especially firefighter and engine use on large fires. Our findings indicate that mobilization is more readily explainable by risk information than demobilization. Our findings also quantified reinforce/release within a region across fire suppression resources in the U.S. and cooperation between regions when sharing a single type of resource from the national pool. Another finding was a stark contrast between demand and risk correlations on high alert days as opposed to normal status days. We are seeing the stress explained in [17] manifest quantitatively as more significant factors occurring in the best-fit risk model. We are left wondering whether a large or small list of viable factors the best way to manage risk. Whatever chaotic effect is causing output noise and model mismatch in our ODE system, it is augmented when the system is on high alert. A pressing question for future policy is: should this circumstance be opposite? Under conditions of high alert and scarce availability ODE models for the allocation data become more complicated. Should a national threat response system refine which risk information layers are salient at high alert by region, lag, and layer? Such a policy might reduce the chaos of high alert making it easier for efficient allocation in which all HMZs get the resources they order. Conversely, it could also lead to decisions based upon incomplete information.

An important nuance is the **(ALL)** and ***(Regional)*** test cases assume that fire demand from the ROSS listings reflect what was used and needed on the fires. To help with this issue, we filter cancelled and unable-to-fill requests using only allocation data that was filled by a resource on a fire. Also, we included ROSS data for reassignments from incident to incident in the computations of $U_{R,G}(t-s)$. This limits the ODE model outputs making them sensitive to ordering mistakes, gaming of the system, or undue holding of certain resources.

Some other limitations to the model include data resolution and availability – for instance, all results for Alaska were jettisoned due to incomplete data streams. This model is focused on demand response and leaves input covariance relatively unmodeled. Replications and statistics were needed to access the parameters, despite the output noise. Sample size limits the confidence of our findings, even adding an additional year's worth of data would better resolve our estimates. Delays are fixed in this model. We elected to do this in accordance with fire resource sharing policy, but other natural hazard applications of ODEs might benefit from testing a more complete list of lags. In addition, our model did not account for the impact of forecast risk information layers. Mechanically, the ODE system built from Eq. (1) can function with an augmented *Lag* set, call it $Lag^* = \{+1,\ 0,\ -1,\ -2,\ -3,\ -7,\ -14,\ -21\}$. Forecast risk weights could be found for $+1$. GIS data for forecasts were not available during development. These limitations and nuances frame a ceiling for how useful the ODE model is to describe resource sharing so we are more interested in taking what we have learned here as baseline for future models.

The results in this paper demonstrate how processing noisy data through the assimilation model can lead to noisy results. However, the strongest signals surpass the noise and validate prior thinking about FFT1s and engines [18,19]. For example, allocation for extended attack on large fires matches our expectations because MODIS fire radiative power data [20] is often significant in the best fit models in our test cases. Stating the model's component equations in general terms helped define specific test cases from the abstract theory. We carried out between $E=1$ and $E=23$ sampling experiments to support our statistical bounds by inverting ill-conditioned matrices and applying $\chi^2_{E-1,0.05}$ statistics to determine significant trends at strong $p < 0.01$ and weak $p \in (0.01, 0.045)$ signals.

We explored the extent to which this inverse problem is ill-conditioned. The CGLS-based inversion method is robust in this regard and trends emerge despite issues in model noise and data mismatch. Even though all results in this paper have been reported from CGLS solutions and deemed weak global least squares minimizer, we found different fit results using Kaczmarz's algorithm. This makes sense because [14] notes this algorithm tends to suffer when tradeoffs in matrix column-data are particularly close. Correlated risk information layers and fire demand data that were central to this paper resist Kaczmarz's algorithm. Since ODE systems are standard math models, these findings suggest a true complexity to the fire allocation problem that may or may not be characteristic of other natural hazard management application areas. We found a stiffer ODE system for the **(California)** test case than the **(Rockies)**. Thus, the ODE model would likely perform better prediction of resource sharing in the latter study area.

Recent consolidation of nonlinear AIMD (Additive Increase Multiplicative Decrease) algorithms in [21] show promise for the ODE system framework established here. Adding a directional aspect to this problem is topic of current research into partial differential equation (PDE) systems. Short et al. [22] demonstrate PDE systems are capable of distinguishing risk-contouring versus risk-following dynamics in a similar demand potential framework. MATLAB PDE software is currently being explored as a finite element method solver on triangular meshes. This would afford simulation en masse and a better understanding of these parameters, but would start with the best fit ODE coefficients.

Future work on this model includes communicating the model and results to an end user group of fire managers, which would rely on the visuals to convey all findings. This research does much to illuminate which indices matter and future work to streamline its interpretability are imperative. In addition, for any resource and region pair we could develop second-stage linear models starting with the significant factors reported in this study. We expect the impact of marginal, convolved factors such as $\partial_t MODIS^* \partial_t BI(t-s)$ in our model would be interesting to discuss with the managers whom also think about risk alignment as simultaneous fires unfold.

5. Conclusion

We elaborated a novel data processing method for resource allocation in multiply connected domains based on a system of ODEs. We showed in theory and practice how to distill resource assignment and risk factor data into a set of linear models. We populated the models with time series data via a smoothed quadrature across individual HMZs. Solutions of our test cases demonstrated how input data covariance in time series GIS data results in noisy parameter estimates. The regression is ill-conditioned in certain models. Despite this issue, we used redundant matrix inversion methodologies based on CGLS to verify the parameter estimates. All our fit results have weakly global minimum residuals for the samples and replicates. We reported best-fit risk coefficients and interpreted their possible meanings for the inverse data problem. Our method was verified by showing known suppression resource movement trends emerge, despite noise in model outputs. We offered the stiffness ratio of the ODE system as a simple characterization of the difficult concepts behind demand coordination on a natural hazard. The research objective for this paper was to quantify risk preferences expressed in natural hazard mitigation resource demand data.

We expect the ODE method is suitable for exhaustive analysis of other multi-region natural hazard resource sharing problems. For example, in terms of flooding [10,11] a large river passing through various jurisdictional zones with their own emergency personnel would meet the basic criteria. Storms [12] would be prime candidates for ODE analysis as extensive GIS weather data along with socio-economic population data could be input through the pipeline of Eqs. (2)–(4). A heat wave [13] would be another natural hazard where if enough data could be amassed, an ODE model might be insightful, but none of these applications have such an alterable natural hazard as wildfire.

Data citations

[Abatzoglou 2013] Abatzoglou, J.T. 2013. Development of gridded surface meteorological data for ecological applications and modelling. Int. J. Climatol. 33, 121–131. https://doi.org/10.1002/joc.3413

[LandScan 2011] This product was made utilizing the LandScan (2011)™ High Resolution global Population Data Set copyrighted by UT-Battelle, LLC, operator of Oak Ridge National Laboratory under Contract No. DE-AC05-00OR22725 with the United State Department of Energy.

[MODIS 2016] MODIS Collection 5 NRT Hotspot / Active Fire Detections MCD14DL. Available on-line [https://earthdata.nasa.gov/firms]. DOI: 10.5067/FIRMS/MODIS/MCD14DL.NRT.005

[NICC.gov/ 2016] National Interagency Coordination Center: Predictive Services and Intelligence. Available on-line [https://www.predictiveservices.nifc.gov/intelligence/intelligence.htm]

[Short 2017] Short, Karen C. 2017. Spatial wildfire occurrence data for the United States, 1992-2015 [FPA_FOD_20170508]. 4th Edition. Fort Collins, CO: Forest Service Research Data Archive. https://doi.org/10.2737/RDS-2013-0009.4

Contemporary policy documents

Interagency Red Book [3] Interagency Coordination and Cooperation: Interagency Standards for Fire and Fire Aviation Operations, NFES 2724 edition, January 2017.

(Mobilization Guide, 2016) National Interagency Mobilization Guide: Geographic Areas. NFES 2092. 1-29; 31-53; 55-56; 81-87, March 2016.

(Preparedness Levels, National Interagency Mobilization Guide, chapter 20) National Preparedness Level Definitions, [Available]: https://www.nifc.gov/fireInfo/fireinfo_prepLevels.html Accessed: 2/27/18.

Supplementary materials

Supplementary material associated with this article can be found, in the online version, at doi:10.1016/j.apm.2018.11.049.

Appendix A. Block assembly of regression matrices/vectorization

The index mapping is a string sort algorithm to connect single index k with the seven-tuple $(r,\ s_1, i,\ g_1, s_2, g_2, s_3)$ to pin down which demand or risk coefficient is in row k in the matrix inversion

$$\{k : x_k \in \vec{\boldsymbol{x}}\} \ \Leftrightarrow\ \left\{(r_1, s_1) : \hat{y}^{s_1}_{r_1} \in \vec{\boldsymbol{y}}\right\} \cup \left\{(i, g_1, s_2) : \hat{a}^{s_2}_{i,g_1} \in \vec{\boldsymbol{a}}\right\} \cup \left\{(g_2, s_3) : \hat{z}^{s_3}_{g_2} \in \vec{\boldsymbol{z}}\right\} \tag{A.1}$$

The block regression inversion system for these models:

$$\boldsymbol{A}_{R,G}\ \vec{\boldsymbol{x}}\ := \begin{bmatrix} \overrightarrow{\boldsymbol{U^s_{r,G}}}^{\boldsymbol{T}}(T_0) & \overrightarrow{\boldsymbol{D^s_{i,g}}}^{\boldsymbol{T}}(T_0) & \overrightarrow{\boldsymbol{U^s_{R,g}}}^{\boldsymbol{T}}(T_0) \\ \vdots & \vdots & \vdots \\ \overrightarrow{\boldsymbol{U^s_{r,G}}}^{\boldsymbol{T}}(t_n) & \overrightarrow{\boldsymbol{D^s_{i,g}}}^{\boldsymbol{T}}(t_n) & \overrightarrow{\boldsymbol{U_{R,g}}}^{\boldsymbol{T}}(t_n) \\ \vdots & \vdots & \vdots \\ \overrightarrow{\boldsymbol{U^s_{r,G}}}^{\boldsymbol{T}}(T_F) & \overrightarrow{\boldsymbol{D^s_{i,g}}}^{\boldsymbol{T}}(T_F) & \overrightarrow{\boldsymbol{U^s_{R,g}}}^{\boldsymbol{T}}(T_F) \end{bmatrix} \begin{Bmatrix} \vec{\boldsymbol{y}} \\ \vec{\boldsymbol{a}} \\ \vec{\boldsymbol{z}} \end{Bmatrix} = \begin{Bmatrix} \frac{dU_{R,G}}{dt}(T_0) \\ \vdots \\ \frac{dU_{R,G}}{dt}(t_n) \\ \vdots \\ \frac{dU_{R,G}}{dt}(T_F) \end{Bmatrix} =:\ \overrightarrow{\partial_t U}_{R,G} \tag{A.2}$$

Each inversion is assembled by flattening the indexed coefficients using (A.1) and concatenating them into a single vector of information $\hat{\boldsymbol{x}} = \{\vec{y}, \vec{a}, \vec{z}\}$ for inversion as a matrix system (A.2).

A.1 Book-keeping example, exercise in combinatorial counting

We write down the three equations used to organize (A.2) based on (A.1) in a $\#G = 3$ size model $g \in \{5, 9, 11\}$ with $|FACTORS| = 26$ risk information inputs with an arbitrary number of resources $\#R$. Such a model was also used in testing. Sharing/cooperative demand impact coefficients for the same resource across other HMZs from (3a) are flattened by lag $s \in Lag(R, G)$, then HMZ g:

$$\overrightarrow{y_{R,G}} := \left\{\ \hat{y}^{s=1}_{g=5}, \hat{y}^1_9, \hat{y}^1_{11}, \ldots, \hat{y}^{|Lag(R,G)|}_5, \hat{y}^{|Lag(R,G)|}_9, \hat{y}^{|Lag(R,G)|}_{11} \right\} \in \mathbb{R}^{3|\aleph|}.$$

Risk coefficients are flattened lag s, then risk factor i, and finally HMZ g:

$$\overrightarrow{a_{R,G}} := \left\{\hat{a}^{s=1}_{i=1,g=5}, \hat{a}^1_{1,9}, \hat{a}^1_{1,11}, \ldots, \hat{a}^1_{26,5}, \hat{a}^1_{26,9}, \hat{a}^1_{26,11}, \ldots, \hat{a}^{|Lag(R,G)|}_{26,5}, \hat{a}^{|Lag(R,G)|}_{26,9}, \hat{a}^{|Lag(R,G)|}_{26,11}\right\} \in \mathbb{R}^{3(26)|Lag(R,G)|}.$$

Reinforce/release demand impact coefficients for other resources with the HMZ flattens by lag s, then resource r

$$\overrightarrow{z_{R,G}} := \left\{\hat{z}^{s=1}_{r=1}, \ldots, \hat{z}^1_R, \ldots, \hat{z}^{|Lag(R,G)|}_1, \ldots, \hat{z}^{|Lag(R,G)|}_R\right\} \in \mathbb{R}^{(\#R-1)|Lag(R,G)|}.$$

These can be checked against the inverse problem sizes and seen in the various visualizations throughout the paper.

Appendix B. Run time and data size analysis

The research code batches three distinct phases: **prepODE.m, setupODE.m**, and **evalODE.m,** runs them in parallel across $\max(\#R, \#G)$. Parallel loops were a speedy way to distribute the computer processing workloads as code was debugged. Each phase works with less data than before. Development involved saving intermediate files; the size of these data dumps for an 18km resolution quadrature with our full suite of risk factors $i_{max} = 45$ was recorded in columns 2 and 4 below

Storage and run-time requirements, ***(Regional Analysis)*** test cases

Phase	Input data size	Run time (*CPU days*)	Output data size	Extra features
prepODE.m	23.3 Gb	14	10.4 Gb	*GIS data visualization risk/demand console*
setupODE.m	10.4 Gb	0.375	494.3 Mb	*Assemble lag structure*
evalODE.m	494.3 Mb	0.006944	4.0 Mb	*Redundant inversion methodologies*

Test case **(ALL)** revealed a memory limit for the model with $\langle \#R = \#G = 12,\ N = 16,\ E = 17\rangle$. This problem was on the CONUS, Alaska, and Hawaii, ground-aerial-command models. On an Intel(R) Core(TM) i7-4770 CPU @ 3.40 GHz with 32 Gb memory, version R2017b of MATLAB was unable to sufficiently compress and save a workable test case **(ALL)**. The data cache of **prepODE.m** was 71.2 Gb in this case. Working with post-processing of results was time consuming, but many open avenues of research are ongoing. ***(Regional Analysis)*** test cases are small so they run quickly and store easily.

References

[1] USDA, The Rising Cost of Fire Operations: Effects on the Forest Service's NonFire Work, 2015. https://www.fs.fed.us/sites/default/files/2015-Fire-Budget-Report.pdf.

[2] D.E. Calkin, K.M. Gebert, J.G. Jones, R.P. Neilson, Forest service large fire area burned and suppression expenditure trends, 1970–2002, J. For. 1034 (2005) 179–183. https://www.fs.usda.gov/treesearch/pubs/24526. Accessed 27 February 2018.

[3] USDOI and USDA, Interagency Standards for Fire and Fire Aviation Operations, 2017. https://www.nifc.gov/PUBLICATIONS/redbook/2017/RedBookAll.pdf.
[4] D.E. Calkin, M.P. Thompson, M.A. Finney, K.D. Hyde, A real-time risk assessment tool supporting wildland fire decisionmaking, J. For. 109 (2011) 274–280, doi:10.1093/jof/109.5.274.
[5] R. Durrett, S. Levin, The importance of being discrete (and spatial), Theor. Popul. Biol. 46 (1994) 363–394, doi:10.1006/tpbi.1994.1032.
[6] H.K. Preisler, A.L. Westerling, K.M. Gebert, F. Munoz-Arriola, T.P. Holmes, Spatially explicit forecasts of large wildland fire probability and suppression costs for California, Int. J. Wildland Fire. 20 (2011) 508–517, doi:10.1071/WF09087.
[7] M.P. Thompson, D.E. Calkin, M.A. Finney, K.M. Gebert, M.S. Hand, A risk-based approach to wildland fire budgetary planning, For. Sci. 591 (2013) 63–77.
[8] F.R. y Silva, J.R.M. Martínez, A. González-Cabán, A methodology for determining operational priorities for prevention and suppression of wildland fires, Int. J. Wildland Fire 23 (2014) 544–554, doi:10.1071/WF13063.
[9] G.J. Cooper, The numerical solution of stiff differential equations, FEBS Lett. 2 (1969) S22–S29, doi:10.1016/0014-5793(69)80072-4.
[10] M. Brilly, M. Polic, Public perception of flood risks, flood forecasting and mitigation, Nat. Hazards Earth Syst. Sci. 5 (2005) 345–355, doi:10.5194/nhess-5-345-2005.
[11] J. Mård, G.D. Baldassarre, M. Mazzoleni, Nighttime light data reveal how flood protection shapes human proximity to rivers, Sci. Adv. 4 (2018) 8.
[12] H. Liu, D.-L. Zhang, Analysis and prediction of hazard risks caused by tropical cyclones in Southern China with fuzzy mathematical and grey models, Appl. Math. Model. 36 (2012) 626–637, doi:10.1016/j.apm.2011.07.024.
[13] Y. Depietri, T. McPhearson, Changing urban risk: 140 years of climatic hazards in New York City, Clim. Change 148 (2018) 95–108, doi:10.1007/s10584-018-2194-2.
[14] R.C. Aster, C.H. Thurber, Parameter Estimation and Inverse Problems, second ed, Academic Press, Waltham, MA, 2013.
[15] J. Li, Y.-T. Chen, Computational Partial Differential Equations Using MATLAB, CRC Press, Boca Raton, 2009.
[16] S. Magnussen, S.W. Taylor, Inter- and intra-annual profiles of fire regimes in the managed forests of Canada and implications for resource sharing, Int. J. Wildland Fire. 21 (2012) 328, doi:10.1071/WF11026.
[17] G. Klein, R. Calderwood, A. Clinton-Cirocco, Rapid Decision Making on the Fire Ground: The Original Study Plus a Postscript, J. Cogn. Eng. Decis. Mak. 4 (2010) 186–209, doi:10.1518/155534310X12844000801203.
[18] E.J. Belval, Y. Wei, D.E. Calkin, C.S. Stonesifer, M.P. Thompson, J.R. Tipton, Studying interregional wildland fire engine assignments for large fire suppression, Int. J. Wildland Fire. 26 (2017) 642–653, doi:10.1071/WF16162.
[19] K.M. Lyon, H.R. Huber-Stearns, C. Moseley, C. Bone, N.A. Mosurinjohn, Sharing contracted resources for fire suppression: engine dispatch in the Northwestern United States, Int. J. Wildland Fire. 26 (2017) 113–121, doi:10.1071/WF16100.
[20] L. Giglio, W. Schroeder, C.O. Justice, The collection 6 MODIS active fire detection algorithm and fire products, Remote Sens. Environ. 178 (2016) 31–41, doi:10.1016/j.rse.2016.02.054.
[21] M.J. Corless, AIMD Dynamics and Distributed Resource Allocation, Society for Industrial and Applied Mathematics, Philadelphia, 2016.
[22] M.B. Short, P.J. Brantingham, A.L. Bertozzi, G.E. Tita, Dissipation and displacement of hotspots in reaction–diffusion models of crime, Proc. Natl. Acad. Sci. USA 107 (2010) 3961–3965, doi:10.1073/pnas.0910921107.